CrossMark

Multi-species trace gas sensing with dual-wavelength QCLs

P. Morten Hundt[1,4] · Béla Tuzson[1] · Oleg Aseev[1] · Chang Liu[1] · Philipp Scheidegger[1] · Herbert Looser[1,3] · Filippos Kapsalidis[2] · Mehran Shahmohammadi[2] · Jérôme Faist[2] · Lukas Emmenegger[1]

Abstract

Instrumentation for environmental monitoring of gaseous pollutants and greenhouse gases tends to be complex, expensive, and energy demanding, because every compound measured relies on a specific analytical technique. This work demonstrates an alternative approach based on mid-infrared laser absorption spectroscopy with dual-wavelength quantum cascade lasers (QCLs). The combination of two dual- and one single-DFB QCL yields high-precision measurements of CO (0.08 ppb), CO_2 (100 ppb), NH_3 (0.02 ppb), NO (0.4 ppb), NO_2 (0.1 ppb), N_2O (0.045 ppb), and O_3 (0.11 ppb) simultaneously in a compact setup (45×45 cm^2). The lasers are driven time-multiplexed in intermittent continuous wave mode with a repetition rate of 1 kHz. The individual spectra are real-time averaged (1 s) by an FPGA-based data acquisition system. The instrument was assessed for environmental monitoring and benchmarked with reference instrumentation to demonstrate its potential for compact multi-species trace gas sensing.

1 Introduction

Environmental trace gas monitoring is of high importance to assess human health risks in polluted urban or industrial environments, and also to efficiently mitigate climate change caused by greenhouse gas emissions. Gaseous pollutants that are to be measured by environmental monitoring stations according to current European regulations are CO, NO_x, SO_2, and O_3 [1]. In addition, some stations monitor further species, e.g., NH_3 and the greenhouse gases CO_2, CH_4, and N_2O [2]. Instruments that are used in environmental

monitoring are based on a wide range of physical measurement principles that target specific compounds. Therefore, monitoring stations usually comprise many different instruments. Correspondingly, they require considerable logistic efforts, technical personnel, and relatively large infrastructure. Moreover, measurements of the important pollutant NO_2 are based on chemiluminescence detection (CLD) of NO, which is an indirect method that relies on catalytic conversion of NO_2, that is known to have cross sensitivities to other nitrogen containing compounds [3, 4].

A highly attractive alternative is offered by direct absorption laser spectroscopy in the mid-infrared spectral region. The wavelength range from 4 to 10 μm has the inherent advantage of containing the fundamental vibrational transition bands of most atmospheric molecules. Highly precise and selective measurements of individual species have already been demonstrated down to ppt (parts per trillion, 10^{-12}) detection limits using quantum cascade lasers (QCLs) [5–7]. The simultaneous detection of all species typically measured in environmental monitoring would, however, require a spectroscopic setup combining a large number of individual laser sources, given the limited tuning range of distributed feedback (DFB)-devices. A first attempt with four QCLs was realized in 2004 to measure four, spectrally separated, species in cigarette smoke [8]. Later studies reported the combination of up to three QCLs within one spectroscopic instrument [9–11]. The

✉ P. Morten Hundt
   Morten.Hundt@empa.ch

1   Empa-Swiss Federal Laboratories for Materials Science and Technology, Laboratory for Air Pollution and Environmental Technology, 8600 Dübendorf, Switzerland

2   ETH Zurich, Quantum Optoelectronics Group, 8093 Zurich, Switzerland

3   FHNW, Institute for Aerosol and Sensor Technology, 5210 Windisch, Switzerland

4   Present Address: MIRO Analytical Technologies GmbH, 8600 Dübendorf, Switzerland

common drawback of these approaches is the increasing complexity of the optics and their sensitivity to mechanical instabilities with the addition of further laser sources. Similarly, the required hardware for controlling each laser temperature and current independently reaches rapidly the practical limits. Thus, the previously discussed combinations of three or more QCLs realized in a single setup led to large instruments with weight > 50 kg, power consumption > 500 W and beyond 12 rack units in 19-in. frames.

These inherent limitations would be greatly reduced in case of broadband laser sources with large spectral coverage. Although, such solutions exist (e.g., EC-QCLs, QCL frequency combs) they are still limited in spectral coverage, power, tuning speed, and stability to allow truly multicomponent, high precision trace gas measurements for long-term monitoring purposes. Recently, considerable efforts have been made to realize on-chip solutions to unify two complementary characteristics in mid-IR sources, namely broad tuning and high spectral resolution. These are realized with electrically tunable DFB devices or arrays of DFB devices. A detailed description of design, fabrication, and performance of the various solutions is given in recent reviews [12–14] and references therein.

In this paper, we adopt the solution of dual-wavelength devices [15, 16] in order to show their suitability for multi-species high-precision trace gas spectroscopy. Such devices—also called dual-section DFBs—consist of two DFB sections, placed on a broad-gain ridge, that emit single mode at two specific target frequencies. Corresponding QCLs were developed for detection of NO and NO_2 in pulsed operation [17] and later for detection of CO, N_2O, and CO_2 in intermittent continuous (iCW) operation [18]. The latter revealed that the dual-section DFB QCL has an inherent etaloning effect, which can be partly suppressed, but requires some additional efforts such as applying anti-reflective coatings. Therefore, a further alternative was realized, also called neighbor DFB, where the two DFBs

are placed about 25 μm apart on the same gain material [19].

In the following, we show that several such dual-wavelength devices can be combined to realize a compact all-in-one environmental trace gas monitor. We present the optical layout, laser driving and data acquisition, discuss the system performance, and demonstrate its application to environmental monitoring.

2 Experimental

2.1 Wavelength selection and dual-wavelength QC lasers

Our measurement strategy for addressing a multitude of gaseous species is to identify spectral regions that contain ro-vibrational transitions of at least two compounds within a typical DFB-QCL tuning range ($\sim$ 1–2 cm^{-1}). Additionally, individual spectral windows should be located in a frequency range that can be covered by broad-gain QCL materials ($\sim$ 300 cm^{-1}). Figure 1 shows an overview of the simulated transitions of the target molecules using the HITRAN 2012 database [20]. Based on a systematic survey of these lines, we identified three particular regions where the above requirements are fulfilled. Table 1 summarizes the five target frequencies along with the corresponding species. These selections represent a good compromise between maximal line-strength, minimal interference from water vapor, and the objective to cover several target molecules within the scanning range of every laser.

The frequencies listed in Table 1 were the targets for the QCL design and are described in more detail within a separate publication in this issue [19].

We chose to combine three different device types for our instrument, namely neighbor DFB, dual-section DFB, and a single-DFB QCL. This gives the possibility to evaluate and

Fig. 1 Simulated absorption of the target gases for typical ambient mole fractions (O_3: 100 ppb; NH_3: 5 ppb; NO_2: 100 ppb; NO: 50 ppb; CO: 150 ppb; N_2O: 330 ppb; CO_2: 400 ppm), considering 76 m optical path length, 80 hPa, and 296 K. The shaded areas mark the frequencies used in this study; the shading colors indicate the three different device types
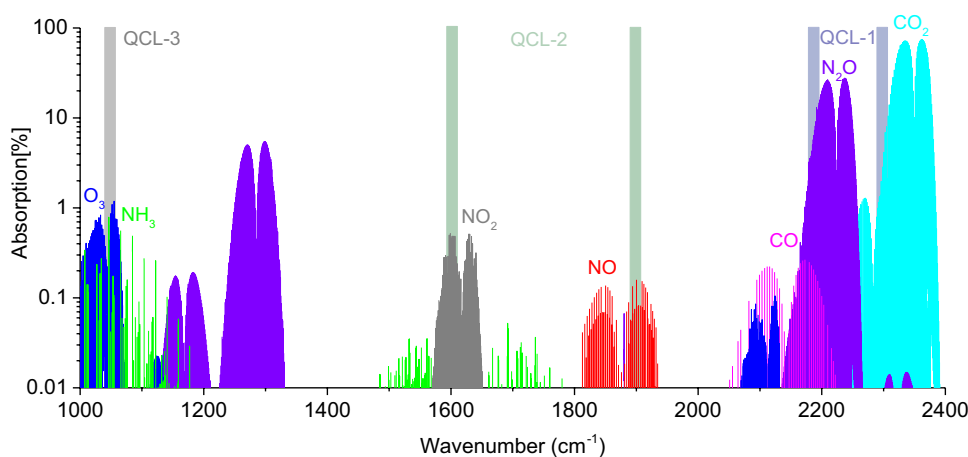
Table 1 Overview of target frequencies, laser device types, and average output powers in iCW mode used for the multi-species gas sensor

Compound	Wavenumbers (cm^{-1})	Device type	Device number	Average Power (mW)
NH_3; O_3	1046.4	Single DFB	QCL-3	7
NO_2	1597.3	Neighbor DFB	QCL-2 (right)	1
NO	1900.0		QCL-2 (left)	0.5
CO; N_2O; H_2O	2190.2	Dual-section DFB	QCL-1 (front)	2
CO_2 (^{12}C and ^{13}C)	2282.9		QCL-1 (rear)	1
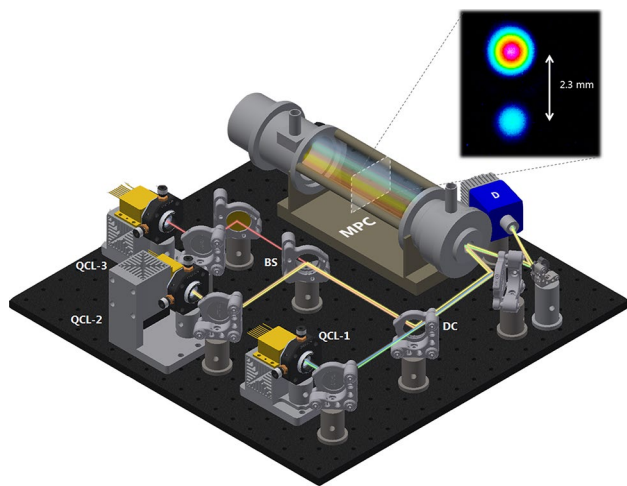
Fig. 2 Model of the optical layout of the multi-laser instrument. The beams of three QCLs are combined using a dichroic (DC) and a CaF$_2$ beam splitter (BS) before the merged beam is coupled into a 76-m-long multipass absorption cell (MPC) and focused on the detector (D). The inset (top-right) shows an IR beam profile of the neighbor DFB QCL (QCL-2) recorded at 55 cm distance, corresponding to the center of the multipass cell

compare the optical properties and the analytical impact of the different approaches.

2.2 Optical layout and beam combination

A schematic of the optical layout for the multi-laser instrument is shown in Fig. 2. The divergent outputs of the QCLs are focused with aspheric lenses ($f = 6$ mm) such that their beam-waist is matched to the multipass cell (AMAC-76, Aerodyne Research Inc.). The beams are combined using a custom dichroic (Lohnstar Optics) optimized to reflect 4 μm and transmit $\lambda > 5$ μm and a wedged CaF$_2$ beam splitter (BSW510, Thorlabs). While the dichroic is optimized for the reflection/transmission of the design wavelengths, the beam splitter causes loss of about 50% of the transmitted/reflected beams. The beam exiting the multipass cell is then focused onto a thermoelectrically cooled MCT detector (PVM-4TE-8, Vigo Systems, S.A.) using a spherical mirror with a focal length of 75 mm.

A major challenge in optimizing the optical alignment in terms of optical fringe level is the two separate output beams of the neighbor DFB-QCL. Although, their spatial separation is as little as 25 μm at the facet, the image at the center of the multipass cell shows a distance of 2.3 mm between the centers of the two beam spots due to the magnification of the optical system (see Fig. 2). Therefore, the apparent width of the dual beam at the entrance to the multipass cell is about the same size as the coupling hole of the cell, which has a diameter of 4.2 mm. Because of this proximity and the Gaussian character of the beams, scattering at the edge of the coupling hole can potentially cause severe interference fringes. Nevertheless, we found the multipass cell being tolerant enough to accept this mismatch in position and beam-waist and allowing for an efficient beam-folding and in/out-coupling of the beams. One key element to achieve good performance in terms of fringe level was to rotate the neighbor DFB-QCL by 90°, i.e., having the DFB-separation perpendicular to the optical plane defined by the multipass cell. This makes the aiming mismatch less critical with respect to the in-coupling angle. Furthermore, a piezoelectric vibrator mounted on the cell's rear mirror is used to randomize the optical fringes and thereby reduce their disturbing effect by spectral averaging [21].

The optical alignment was optimized based on real-time inspection of the laser beam size and position by using an infrared beam profiler (WinCamD-IR-BB, DataRay Inc.). The insert in Fig. 2 shows an example of the beam profile for the neighbor DFB-QCL measured at the center of the multipass cell corresponding to 55 cm distance from the source. The intensity difference is due to the difference in output power of the two DFBs.

2.3 Laser driving and data acquisition

The laser driving and data acquisition system used for this study is described in detail by Liu et al. [22] and thus, we only briefly review the functionalities of the system and its application for driving several multi-wavelength lasers and the associated data acquisition.

The impact of driving electronics noise on the spectral properties of QCLs has been investigated by several

publications (see, e.g., Tombez et al. [23] and references therein). Estimating the laser linewidth (FWHM) as a function of the driver current noise spectral density, it was shown that a current noise of about 1 nA/Hz$^{1/2}$ is needed before the intrinsic properties of QCLs are observed. Commercially available solutions fulfilling this requirement are still bulky devices with large heat dissipation. Obviously, combining many, in our case five, such drivers to drive multiple lasers would rapidly jeopardize the compactness of any setup. To overcome this limitation, we developed a more compact laser driver based on the concept of intermittent continuous wave (iCW) driving [24]. This approach leads to a compact, yet a flexible laser driver that eliminates the need for any external electronics (e.g., function generator or DAQ) for current modulation while maintaining a high modulation capability (up to 20 kHz), and considerably lowers the demands on power supply performance. Using the iCW driving it is possible to completely decouple the driver from the external power supply during laser operation. The laser current is solely provided by the charge stored in capacitors and also results in heat dissipation of less than 5 W for driving the five lasers. This especially facilitates the encapsulation of QCL devices into compact packages such as HHL or even TO-3. The current noise level of this laser driver was demonstrated to be better than 1 nA/Hz$^{1/2}$. Moreover, the driver supports operating a wide range of multi-wavelength QCL device types and allows stacking for the purpose of multiple laser configurations. Its adaptation to the various driving situations is supported by numerous FPGA functionalities that were implemented on the system-on-chip (SoC), such as flexible generation of a large variety of synchronized trigger signals and digital IOs. The same SoC is used to sample the spectroscopic signal at rates up to 125 MS/s with 14-bit resolution.

The system can support up to six lasers operated in a time-multiplexed iCW driving scheme with a single detector [24]. The lasers are triggered in a predefined sequence with a total period of 1 ms, while the pulse duration for each laser (-section) can be set individually with a time resolution of 8 ns. For our setup, the dual-wavelength devices were operated with 25 µs pulse duration, while the single-DFB device at 9.6 µm was driven with 50 µs current pulses. During such a current pulse, the QCL heats up and therefore tunes rapidly in frequency. The lasers are completely turned off during the remaining time to lower the overall power consumption and hence to reduce the cooling requirements. This results in a duty-cycle of 2.5 and 5% for the dual- and single-DFB QCLs, respectively. The spectra of each QCL are recorded by the FPGA-based data acquisition. Additionally, the detector zero level signal is measured for 5 µs at the beginning of each cycle and is used for spectral normalization.

The spectra are averaged in real-time by the FPGA and then transferred to a PC for spectral analysis by a custom written LabVIEW program. The FPGA system is also used to provide the full control of the spectrometer by reading out pressure and temperature values or setting laser temperatures and valve positions.

2.4 Site and sampling for environmental monitoring

Ambient air measurements of all parameters were performed in our laboratory at Empa (Dübendorf, Switzerland) for several days in early December 2017, linked to calibration standards and compared to standard air quality monitoring equipment. The location is suburban, densely populated and impacted by emissions from a close-by motorway.

We used a membrane pump (N920G, KNF) to constantly draw ambient air from outside through a PTFE tube of 10 m length and 4 mm inner diameter to the multipass cell of the laser spectrometer. The pressure in the cell was maintained at 75 hPa by using a needle valve in the up-stream flow resulting in a gas flow of 1 l/min through the cell. A solenoid valve was used to switch periodically—once per hour for 5 min—between ambient air and calibrated reference gas. The calibration gas was free of NO, NO_2, NH_3, and O_3 and was previously calibrated for mole fractions of CO (114.12 $\pm$ 0.25 ppb), CO_2 (400.17 $\pm$ 0.02 ppm) and N_2O (322.77 $\pm$ 0.09 ppb) using commercial cavity ring-down spectrometers (G1301 and G5310, Picarro Inc.). These periodic measurements of calibration/zero gas were used to correct for instrument drifts, which were mainly caused by ambient temperature variations. The measurements of NO and NO_2 were compared to a commercial dual channel chemiluminescence detector (CLD) measuring NO and NO_x (APNA 360, Horiba), sharing the air inlet with the laser spectrometer. Other species (CO_2, CO, O_3) were compared to the measurements of the Dübendorf air quality monitoring site of the Swiss National Air Pollution Monitoring Network (NABEL) situated about 130 m from our sampling inlet. At the NABEL station, CO_2 is monitored with a cavity ring-down spectrometer (G1301, Picarro Inc.), CO is measured by non-dispersive IR absorption (APMA 370, Horiba) and O_3 by UV-absorption (49i, Thermo). Details about these measurements and their uncertainties can be found in the NABEL technical report [25]. N_2O could not be compared directly to an alternative measurement technique; however, we verified our results by comparing to the reference gas bottle with NH_3-free air and a known N_2O mole fraction (322.77 $\pm$ 0.09 ppb). For NH_3, stable reference gases are difficult to produce and no direct comparison was available.

3 Results and discussion

3.1 Instrument characterization

The mole fractions were retrieved from the raw data by real-time least-square fitting of the transmission signals to a Voigt profile. The fitting model is based on spectral parameters taken from the HITRAN database [20] and experimental parameters such as optical path length, gas temperature, and pressure. The tuning rate of each QCL is obtained by inserting a 2-in. Germanium etalon with a free spectral range of 0.0244 cm^{-1} (at 5 µm and 25 °C) in the laser beam path. Figure 3 shows the normalized and fitted spectra for the five wavelength regions that are used by the spectrometer.

We assessed the instrument performance by measuring constant mole fractions of the target gases and applying an Allan–Werle variance analysis [26] to the retrieved values. For NO, NO_2, O_3, and NH_3 we used zero-air and for CO_2, N_2O, and CO a pressurized gas cylinder with mole fractions of CO_2 (400 ppm), N_2O (323 ppb) and CO (114 ppb). Figure 4 shows the Allan–Werle deviation plots for the gases mentioned above. Table 2 summarizes the results along with the corresponding absorption noise. The values reported here are up to 50 times higher than currently achievable noise levels in comparable single laser QCLAS instruments with reported absorption noise of $\sim 5 \times 10^{-6}$ at 1 s average and $\sim 5 \times 10^{-7}$ at the Allan-minimum (about 100 s averaging) [5]. The significantly higher noise level for CO_2 can be explained by a very strong absorption ($> 40\%$), and changes in laboratory air CO_2 mole fraction which impact the (unflushed) optical setup. Nevertheless, the CO_2 detection limit is below the GAW extended compatibility goal of ± 0.2 ppm [27]. The Allan–Werle analysis revealed no particular difference between the performance of dual-section device (QCL-1), the neighbor DFB (QCL-2), and the single DFB (QCL-3). The differences in achievable precision within our system and in comparison to state-of-the-art instrumentation can be mostly explained by other effects. We observed, for instance, that N_2O averages much better (up to 1000 s) than CO (100 s) despite being measured with the same section of the dual-section QCL. In that case, the averaging of CO is likely to be influenced by concentration changes outside the multipass cell.

The discrepancy between our setup and comparable single laser QCLAS instruments is mostly caused by a relatively high detector noise level, which has several reasons: (1) multiple lasers are combined with wavelengths from 4 to 10 µm and, therefore, a broadband IR-detector with large active area (1 mm^2) without immersion lens is needed, which has a D^* (detectivity) up to two orders of magnitude lower than a detector optimized, e.g., for
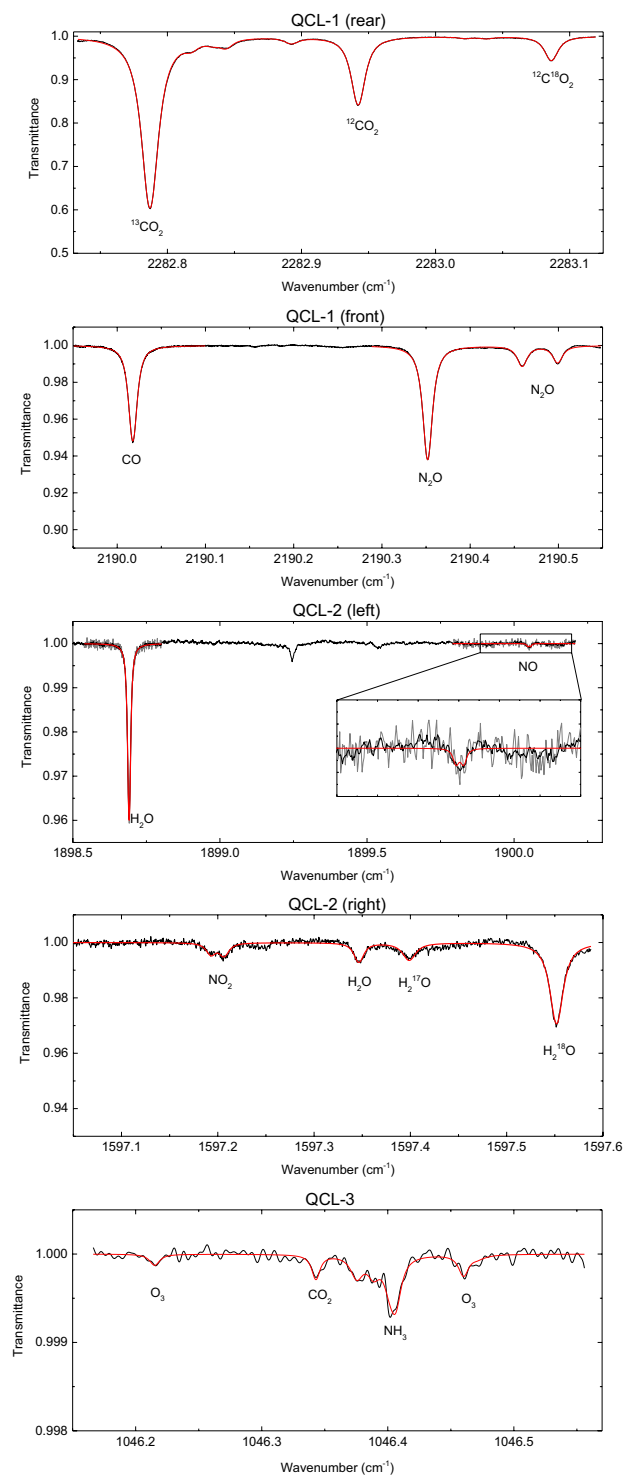

Fig. 3 Normalized and fitted transmission spectra of the five wavelength regions covered by the QCLs. The Voigt-fit is shown in red, while the black line indicates the measured spectrum averaged over 1000 scans, i.e., for 1 s. An exception is the NO spectrum, where the black line depicts an average of 20,000 spectra and the gray line is an average of 1000 spectra. All spectra were recorded at a pressure of 75 hPa, $T = 25$ °C and 76 m optical path length. The mole fractions were as follows (given in brackets): CO_2 (430 ppm), CO (200 ppb), N_2O (327 ppb), H_2O (0.7%), NO (14 ppb), NO_2 (27 ppb), NH_3 (5 ppb), O_3 (15 ppb)
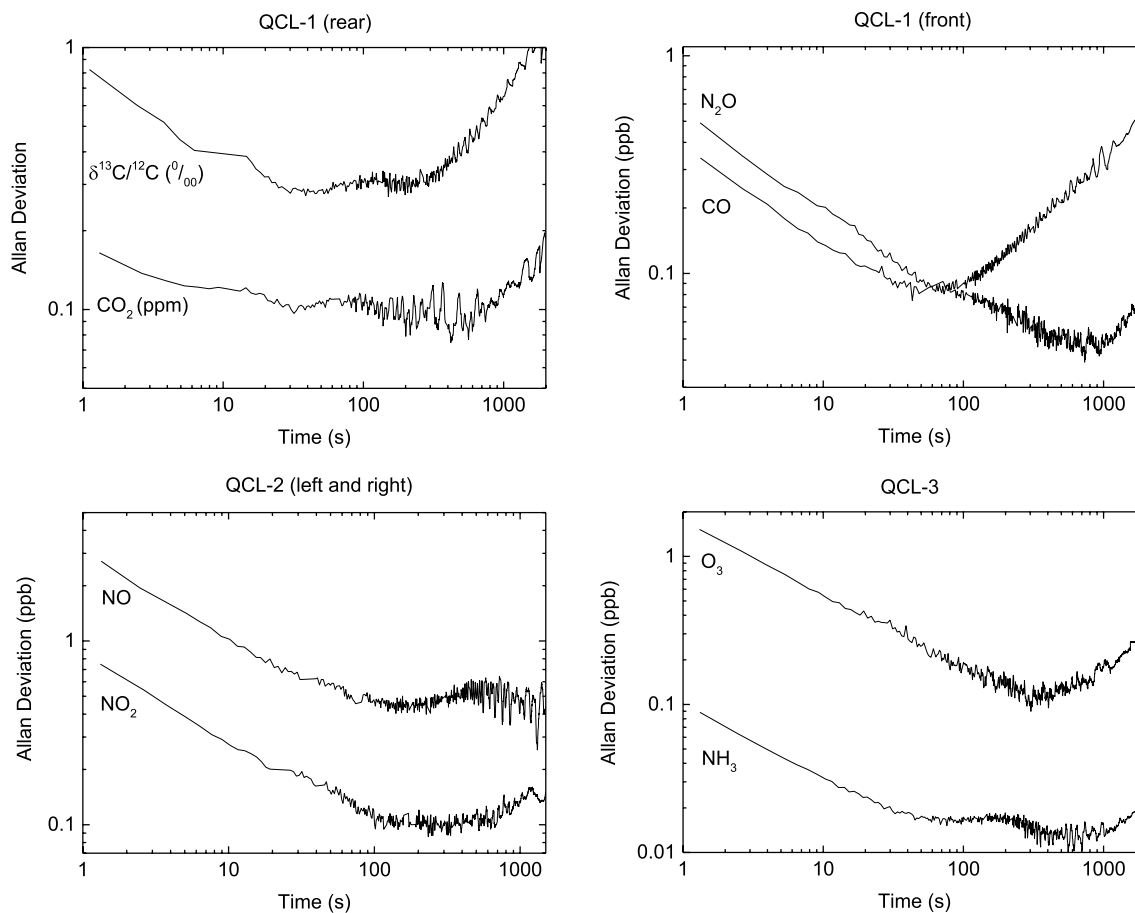
Fig. 4 Allan–Werle deviation plots for the measured gas species. For NO, NO_2, O_3, and NH_3 zero-air was measured, while in the case of CO_2, N_2O, and CO pressurized air was used

Table 2 Summary of Allan–Werle deviations representing the 1σ limit of detection and the corresponding absorption noise given after 1 s integration time and at the Allan deviation minimum ("best"), which was typically reached between 100 and 300 s integration time

Species	Precision (ppb)		Absorption noise		DFB-QCL type	Device number
	1 s	Best	1 s	Best		
CO	0.35	0.08	9.2E−05	2.1E−05	Dual-section	QCL-1 (front)
N_2O	0.49	0.045	9.9E−05	9.0E−06	Dual-section	QCL-1 (front)
CO_2	170	100	1.6E−04	9.3E−04	Dual-section	QCL-1 (rear)
$\delta^{13}CO_2$ [‰]	0.9	0.28	–	–	Dual-section	QCL-1 (rear)
NO	3	0.4	1.7E−04	2.2E−05	Neighbor	QCL-2 (left)
NO_2	0.8	0.1	1.6E−04	2.0E−05	Neighbor	QCL-2 (right)
O_3	1.7	0.11	3.2E−05	2.0E−06	Single	QCL-3
NH_3	0.1	0.016	3.0E−05	4.8E−06	Single	QCL-3

The numbers shown for $\delta^{13}CO_2$ are given in ‰

3–6 μm wavelength. (2) The lasers are still prototype devices that cannot compete with the performance of commercial devices neither in terms of optical power (~ 1 mW) nor emission properties. (3) There is a difference in integration time/duty-cycle leading to a lower number of spectra that can be averaged per time: whilst a single laser instrument can be operated at a duty-cycle close to 100%, the multi-species instrument is time multiplexed between five lasers resulting in a much lower duty-cycle (see above) per laser device. (4) The data acquisition has a high bandwidth (125 MHz) required for the faster tuning of the QCLs in iCW driving and is therefore more susceptible for high-frequency noise.

In addition, to realize a compact optical layout, compromises were made on the optics and coupling of the laser beams to the multipass cell. We used fast optics for direct focusing of the QCL outputs to the multipass cell. This leads to chromatic aberration (in case of the dual-lasers), and therefore a compromise in focal position/beam-waist size in the multipass cell. Furthermore, the fact that the neighbor DFB produces two separate beams that are 2.3 mm apart at the center of the cell leads to imperfect beam propagation and scattering on the coupling hole of the cell. These compromises can influence the achievable fringe level. However, our results indicate that the measurement precision is mainly limited by detector noise. Consequently, those lasers with the lowest output power (Table 1) exhibit the highest absorption noise levels (see Table 2).

Despite the fact that QCLAS is, in principle, an absolute analytical technique, calibrations were performed in order to improve the accuracy of the instrument. Table 3 shows a summary of the calibration factors that were applied. CO, N_2O, CO_2, and NO were calibrated to reference gases and show only small deviations of $< 5\%$ which is in the range of the uncertainty of the spectroscopic parameters of the HITRAN database [20]. Since NO_2 calibration gases are difficult to obtain and tend to be unstable, NO_2 was calibrated during ambient air measurements to a CLD (APNA 360, Horiba), which is the reference method for NO_2 monitoring

according to regulatory norm [1]. The calibration factor is likely to be overestimating the true NO_2 mole fraction, because CLDs using catalytic converters have cross sensitivities to other nitrogen containing compounds [3, 4]. Since O_3 and NH_3 are also unstable, calibration gases are not available or not reliable. Therefore, the NH_3 measurement was not calibrated, but a conservative estimate of $\pm 20\%$ was made based on the uncertainty of the line strengths of 10–20% stated in the HITRAN database [20].

In the case of O_3 we calibrated our spectrometer using a UV-absorption instrument (Thermo 49i-PS), which serves as a transfer standard for regular quality control at the stations of the NABEL network. The instrument uses a dual-cell photometer to produce constant O_3 mole fractions with a UV-lamp, and it is traceable to a standard reference photometer produced by NIST [25]. Its uncertainty results from the combination of the uncertainties of the reference standard and the UV photometer itself; it is less than 1% of the mole fraction reading for mole fractions < 250 ppb.

We measured O_3 from the UV photometric standard with the QCLAS while stepwise increasing the concentration (Fig. 5a). The obtained scatter plot is shown in Fig. 5b, where the measured QCLAS mole fraction (4 min mean with 2σ error bars) is plotted over the set mole fraction of the transfer standard (2σ error bars). The measured zero-air values of the QCLAS showed an offset of about 7 ppb (caused by interference fringes) and a total drift of $+2$ ppb during the course of the experiment (1 h). We corrected for this drift by linear interpolation between the first and the last zero-air measurements and subtraction of the offset. The resulting scatter-plot shows an excellent linearity ($R^2 = 0.9995$) for the instrument over the whole concentration span covering the range expected in environmental monitoring. However, the slope deviates by about 10% from unity. As mentioned above, this mismatch can partly be explained by the uncertainty of the HITRAN database, as it states uncertainties between 2 and 5% (where stated) for the line-intensities of O_3 in the respective wavelength region [20]. Finally, some

Table 3 Summary of calibration factors for the QCLAS

Species	Calibration factor	Source for calibration	Device number
CO	1.01	Ref. gas	QCL-1 (front)
N_2O	1.05	Ref. gas	QCL-1 (front)
CO_2	1.02	Ref. gas	QCL-1 (rear)
NO	0.99	Ref. gas	QCL-2 (left)
NO_2	1.08	Horiba, APNA 360	QCL-2 (right)
O_3	1.1	Thermo, 49i-PS	QCL-3
NH_3	1.0 ± 0.2[a]	n.a	QCL-3

[a]Estimated

Fig. 5 **a** Stepwise changes in O_3 produced by NABEL transfer standard (Thermo 49i-PS) in red and measured by the QCLAS with 1 s time resolution (black line). A linear offset and drift correction was already applied. **b** Scatter-plot of the averaged mole fraction steps measured by QCLAS vs. O_3 reference values
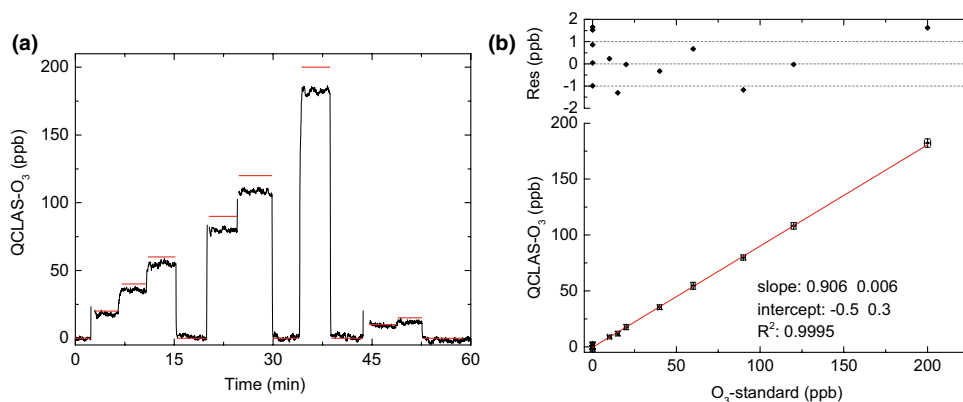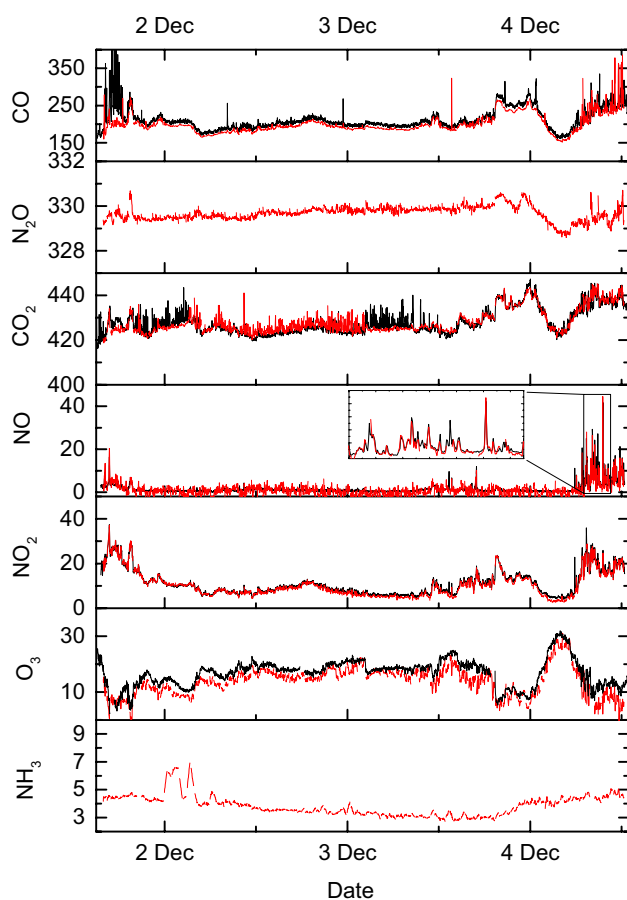
Fig. 6 Time series of mole fractions measured by QCLAS (red traces) and reference instruments (black traces, where available). Mole fraction units are ppb (ppm for CO_2). All data are 1 min averages. For the QCLAS data, correction factors/calibrations listed in Table 3 were considered and the hourly drift correction was applied

degree of O_3 dissociation on the aluminum body of the multipass cell of the QCLAS can be expected as well.

3.2 Measurement of ambient air at Empa/ Dübendorf

A short feasibility field-campaign of a few days was realized to demonstrate the instrument's capability for environmental monitoring. Figure 6 shows the recorded time series of seven greenhouse gases and pollutants simultaneously measured in Dübendorf (Switzerland) in early December 2017. The previously determined calibration factors and the described drift correction were applied. The measurement period started on a Friday and ended on a Monday, therefore, emissions from the rush-hours can be observed.

Despite the spatial separation of the gas inlets between our laboratory and the NABEL station, we see very good agreement for the CO and CO_2 measurements. Differences are well within the range that would be expected due to the

local variability and different exposure to emissions from road traffic. The discrepancy for O_3 may appear slightly higher but, O_3 is known to be very reactive, and as such, strong local gradients can be expected. In fact, the lower concentrations of the QCLAS are consistent with its smaller distance to the road traffic.

For the case, where the instruments share the same air inlet, i.e., for the NO and NO_2, the QCLAS measurements agree well with the CLD in the laboratory. Although, N_2O and NH_3 were not compared to reference instruments, the retrieved mole fractions are within the expected values for a suburban site such as Dübendorf. The N_2O is at the global background level of 329 ppb with small variations of ± 1 ppb. The fast variations at the end of the time series are likely to be caused by emissions from road traffic. Finally, NH_3 is at the expected level of 3–5 ppb.

4 Conclusion

The development and validation of a compact laser spectroscopic setup as a universal solution for simultaneous measurement of the most important greenhouse gases and pollutants was described. The technique relies on state-of-the-art dual-wavelength DFB-QCL devices. Two different designs, dual-section and neighbor DFB-QCL devices, were employed to investigate their suitability for high-precision laser absorption spectroscopic applications. A dedicated hardware and software solution was employed, with compactness and low overall power consumption as key factors, supporting time-multiplexed iCW operation of multiple dual-DFB QCL devices, and to provide real-time spectral analysis of up to nine different target species. The hardware supports up to six lasers with a single multipass cell and a single detector.

The data quality was assessed by Allan–Werle variance analyses and by comparing to standard air quality monitoring equipment, where available. The achieved precisions and detection limits are sufficient for air quality monitoring and other atmospheric science applications.

Further extension of the target species can easily be realized, e.g., by replacing the single-DFB QCL at 9.6 µm with a dual-wavelength DFB-QCL for covering the frequency around 1352 cm^{-1} to measure CH_4 and SO_2 [19]. This would complete the instrument to be a true all-in-one environmental monitoring station, opening a wide range of new possibilities in atmospheric sciences.

was indispensable for this work. Christoph Zellweger (Empa) is acknowledged for providing the calibrated reference gas cylinder.

References

1. EU, in *Directive 2008/50/EC of the European Parliament and of the Council of 21 May 2008 on ambient air quality and cleaner air for Europe* (Official Journal of the European Union, 2008). http://data.europa.eu/eli/dir/2008/50/oj
2. WMO/GAW WMO Global Atmosphere Watch (GAW), Implementation plan: 2016–2023, WMO (2016), http://www.wmo.int/pages/prog/arep/gaw/gaw-reports.html. Accessed 16 May 2018
3. M. Steinbacher, C. Zellweger, B. Schwarzenbach, S. Bugmann, B. Buchmann, C. Ordóñez, A.S.H. Prevot, C. Hueglin, Nitrogen oxide measurements at rural sites in Switzerland: bias of conventional measurement techniques. J. Geophys. Res. Atmos. **112**, D11307 (2007)
4. E.J. Dunlea, S.C. Herndon, D.D. Nelson, R.M. Volkamer, F. San Martini, P.M. Sheehy, M.S. Zahniser, J.H. Shorter, J.C. Wormhoudt, B.K. Lamb, E.J. Allwine, J.S. Gaffney, N.A. Marley, M. Grutter, C. Marquez, S. Blanco, B. Cardenas, A. Retama, C.R. Ramos Villegas, C.E. Kolb, L.T. Molina, M.J. Molina, Evaluation of nitrogen dioxide chemiluminescence monitors in a polluted urban environment. Atmos. Chem. Phys. **7**, 2691–2704 (2007)
5. J.B. McManus, M.S. Zahniser, D.D. Nelson, J.H. Shorter, S.C. Herndon, D. Jervis, M. Agnese, R. McGovern, T.I. Yacovitch, J.R. Roscioli, Recent progress in laser-based trace gas instruments: performance and noise analysis. Appl. Phys. B Lasers Opt. **119**, 203–218 (2015)
6. J.B. McManus, M.S. Zahniser, D.D. Nelson Jr., J.H. Shorter, S. Herndon, E. Wood, R. Wehr, Application of quantum cascade lasers to high-precision atmospheric trace gas measurements. Opt. Eng. **49**, 111124 (2010)
7. B. Tuzson, K. Zeyer, M. Steinbacher, J.B. McManus, D.D. Nelson, M.S. Zahniser, L. Emmenegger, Selective measurements of NO, NO$_2$ and NO$_y$ in the free troposphere using quantum cascade laser spectroscopy. Atmos. Meas. Tech. **6**, 927–936 (2013)
8. R.E. Baren, M.E. Parrish, K.H. Shafer, C.N. Harward, S. Quan, D.D. Nelson, J.B. McManus, M.S. Zahniser, Quad quantum cascade laser spectrometer with dual gas cells for the simultaneous analysis of mainstream and sidestream cigarette smoke. Spectrochim Acta Part A Mol Biomol. Spectrosc. **60**, 3437–3447 (2004)
9. M. Huebner, S. Welzel, D. Marinov, O. Guaitella, S. Glitsch, A. Rousseau, J. Roepcke, TRIPLE Q: A three channel quantum cascade laser absorption spectrometer for fast multiple species concentration measurements. Rev. Sci. Instrum. **82**, 092102 (2011)
10. C.L. Schiller, H. Bozem, C. Gurk, U. Parchatka, R. Königstedt, G.W. Harris, J. Lelieveld, H. Fischer, Applications of quantum cascade lasers for sensitive trace gas measurements of CO, CH$_4$, N$_2$O and HCHO. Appl. Phys. B **92**, 419–430 (2008)
11. V. Catoire, C. Robert, M. Chartier, P. Jacquet, C. Guimbaud, G. Krysztofiak, The SPIRIT airborne instrument: a three-channel infrared absorption spectrometer with quantum cascade lasers for in situ atmospheric trace-gas measurements. Appl. Phys. B **123**, 244 (2017)
12. M. Razeghi, W.J. Zhou, S. Slivken, Q.Y. Lu, D.H. Wu, R. McClintock, Recent progress of quantum cascade laser research from 3 to 12 mum at the Center for Quantum Devices Invited. Appl. Opt. **56**, H30-H44 (2017)
13. P. Rauter, F. Capasso, Multi-wavelength quantum cascade laser arrays. Laser Photonics Rev. **9**, 452–477 (2015)
14. M. Süess, R. Peretti, Y. Liang, J. Wolf, C. Bonzon, B. Hinkov, S. Nida, P. Jouy, W. Metaferia, S. Lourdudoss, M. Beck, J. Faist, Advanced fabrication of single-mode and multi-wavelength MIR-QCLs. Photonics **3**, 26 (2016)
15. A. Straub, C. Gmachl, D.L. Sivco, A.M. Sergent, F. Capasso, A.Y. Cho, Simultaneously at two wavelengths (5.0 and 7.5 mum) single-mode and tunable quantum cascade distributed feedback lasers. Electron. Lett. **38**, 565–567 (2002)
16. J. Jagerska, P. Jouy, A. Hugi, B. Tuzson, H. Looser, M. Mangold, M. Beck, L. Emmenegger, J. Faist, Dual-wavelength quantum cascade laser for trace gas spectroscopy. Appl. Phys. Lett. **105**, 161109 (2014)
17. J. Jagerska, P. Jouy, B. Tuzson, H. Looser, M. Mangold, P. Soltic, A. Hugi, R. Broennimann, J. Faist, L. Emmenegger, Simultaneous measurement of NO and NO$_2$ by dual-wavelength quantum cascade laser spectroscopy. Opt. Express **23**, 1512–1522 (2015)
18. M. Süess, P.M. Hundt, B. Tuzson, S. Riedi, J. Wolf, R. Peretti, M. Beck, H. Looser, L. Emmenegger, J. Faist, Dual-section DFB-QCLs for multi-species trace gas analysis, Photonics **3**, 24 (2016)
19. F. Kapsalidis, M. Shahmohammadi, M. Süess, J.M. Wolf, E. Gini, M. Beck, M. Hundt, B. Tuzson, L. Emmenegger, J. Faist, Dual-wavelength DFB quantum cascade lasers: sources for multi-species trace gas spectroscopy. Appl. Phys. B Lasers Opt. (2018). https://doi.org/10.1007/s00340-018-6973-2 (**this issue**)
20. L.S. Rothman, I.E. Gordon, Y. Babikov, A. Barbe, D.C. Benner, P.F. Bernath, M. Birk, L. Bizzocchi, V. Boudon, L.R. Brown, A. Campargue, K. Chance, E.A. Cohen, L.H. Coudert, V.M. Devi, B.J. Drouin, A. Fayt, J.M. Flaud, R.R. Gamache, J.J. Harrison, J.M. Hartmann, C. Hill, J.T. Hodges, D. Jacquemart, A. Jolly, J. Lamouroux, R.J. Le Roy, G. Li, D.A. Long, O.M. Lyulin, C.J. Mackie, S.T. Massie, S. Mikhailenko, H.S.P. Mueller, O.V. Naumenko, A.V. Nikitin, J. Orphal, V. Perevalov, A. Perrin, E.R. Polovtseva, C. Richard, M.A.H. Smith, E. Starikova, K. Sung, S. Tashkun, J. Tennyson, G.C. Toon, V.G. Tyuterev, G. Wagner, The HITRAN2012 molecular spectroscopic database. J. Quant. Spectrosc. Radiat. Transf. **130**, 4–50 (2013)
21. J.B. McManus, D.D. Nelson, S.C. Herndon, J.H. Shorter, M.S. Zahniser, S. Blaser, L. Hvozdara, A. Muller, M. Giovannini, J. Faist, Comparison of cw and pulsed operation with a TE-cooled quantum cascade infrared laser for detection of nitric oxide at 1900 cm^{-1}. Appl. Phys. B **85**, 235–241 (2006)
22. C. Liu, B. Tuzson, P. Scheidegger, H. Looser, B. Bereiter, M. Graf, M. Hundt, O. Aseev, D. Maas, L. Emmenegger, Laser driving and data processing concept for mobile trace gas sensing: design and implementation. Rev. Sci. Instrum. (2018, to appear)
23. L. Tombez, J. Di Francesco, S. Schilt, G. Di Domenico, J. Faist, P. Thomann, D. Hofstetter, Frequency noise of free-running 4.6 um distributed feedback quantum cascade lasers near room temperature. Opt. Lett. **36**, 3109–3111 (2011)
24. M. Fischer, B. Tuzson, A. Hugi, R. Broennimann, A. Kunz, S. Blaser, M. Rochat, O. Landry, A. Mueller, L. Emmenegger, Intermittent operation of QC-lasers for mid-IR spectroscopy with low heat dissipation: tuning characteristics and driving electronics. Opt. Express **22**, 7014–7027 (2014)
25. NABEL, Technischer Bericht zum Nationalen Beobachtungsnetz für Luftfremdstoffe (NABEL), (2017). https://www.bafu.admin.ch/bafu/de/home/themen/luft/zustand/daten/nationales-beobachtungsnetz-fuer-luftfremdstoffe--nabel-.html. Accessed 16 May 2018
26. P. Werle, R. Mucke, F. Slemr, The limits of signal averaging in atmospheric trace-gas monitoring by tuneable diode-laser absorption-spectroscopy (TDLAS). Appl. Phys. B Photophys. Laser Chem. **57**, 131–139 (1993)
27. WMO/GAW, 18th WMO/IAEA Meeting on Carbon Dioxide, Other greenhouse gases and related tracers measurement techniques (GGMT-2015), WMO (2015), https://library.wmo.int/opac/doc_num.php?explnum_id=3074. Accessed 16 May 2018